Technical Note

Fundamentals of magnetic field measurement with NV centers in diamond

Related products: Qnami ProteusQ™, Quantilever™MX

Release date: 07 December 2020

At one glance

The present technical note aims to provide the reader with the fundamentals of NV magnetometry. In a first part we introduce the nitrogen-vacancy (NV) center and its fundamental properties. In the second part we show how the NV center is used to measure magnetic fields with unprecedented sensitivity.

1 The NV center

The NV center is a point defect in the diamond lattice where two adjacent carbon atoms are substituted by a nitrogen atom and a vacancy, respectively (cf. Fig. 1). The complex forms 4 covalent bonds with the surrounding carbon atoms leaving one electron from the nitrogen atom unpaired. The result is a system presenting a spin 1/2, denoted as NV^0. The NV^0 configuration modifies the energy distribution within the crystal structure in such a way that it allows the NV center to trap an additional free-floating electron from the conduction band (CB) forming the negatively charged complex NV^- [1]. The negatively charged state of the NV center provides the rich toolkit that is at the root of NV magnetometry applications. For simplicity, we refer below with the term 'NV center' to the negatively charged configuration.

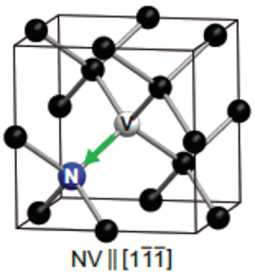

Fig. 1: The NV center in a diamond unit cell. Two adjacent carbon atoms are replaced by a nitrogen atom and a vacancy. The resulting symmetry axis along the [111] direction of the diamond lattice defines the quantization axis of the system and is referred to as the z-axis (green arrow).

1.1 Energy level diagram of the NV center

Fig. 2a presents a simplified energy level diagram of the NV center which consists of a ground state $|g\rangle$, an excited state $|e\rangle$, and a shelving state $|s\rangle$, all within the 5.5 eV wide diamond band gap. In the absence of any external field, the ground state $|g\rangle$ is split into two magnetic spin levels, the $|m_S = 0\rangle$ and the $|m_S = \pm 1\rangle$ states. In the course of this note, we will drop the m_s label for the spin quantum number for reasons of brevity and utilize instead numbers for the associated spin states. These two spin states are separated by a zero-field splitting (ZFS) $D_G = 2.87$ GHz - a consequence of the spin-spin interaction between the electrons of

the NV center due to a tight confinement within the non-cubic diamond lattice. The excited state $|e\rangle$ of the NV center presents a similar structure. We note the smaller ZFS parameter, D_E, resulting from the contribution of a second interaction term associated with spin-orbit coupling in the excited state [1]. The third state $|s\rangle$ represents a shelving state stemming from the intrinsic electronic configuration of the NV center.

1.2 Optical properties of the NV center

Upon excitation with a green laser, electrons are transferred from the ground to the excited state (cf. Fig. 2a). Remarkably, this non-resonant process remains spin-conserving so that electrons from the $|0, g\rangle$ ($|\pm 1, g\rangle$) state end up in the $|0, e\rangle$ ($|\pm 1, e\rangle$) state. In both cases the electron may decay back to the ground state by emitting a red photon. This fluorescence property is evidenced in Fig. 2b, which shows a photoluminescence map of a diamond crystal, where every bright spot corresponds to the fluorescence of a single NV center. At room temperature, this direct optical transition is accompanied by phonon assisted recombinations (known as the phonon sideband, PSB), which produce a fluorescence band comprised between 600 and 850 nm (cf. Fig.2c). A further feature is the extreme photostability over time of the defect making it an excellent, non-bleaching single photon source.

In addition to the radiative channels, electrons in the $|\pm 1, e\rangle$ state may decay non-radiatively (branching ratio $\approx 30\,\%$) through the shelving state $|s\rangle$, ending up predominantly in $|0, g\rangle$. This has two fundamental consequences, which are at the root of quantum sensing and quantum computing applications: 1) the ability to initialize the NV center in a well-defined spin state and 2) the possibility to read-out its spin state optically.

1.3 Initialization of the spin-state

In a continuous wave measurement, the additional decay path from $|\pm 1, e\rangle$ to $|0, g\rangle$ through the long lived shelving state $|s\rangle$ (lifetime of 300 ns vs. 13 ns for the excited state) impacts the population of the ground state $|g\rangle$. On the one hand, electrons from the $|0, g\rangle$ and $|\pm 1, g\rangle$ return to their initial states after a radiative cycle, but on the other hand, the presence of this additional decay mechanism eventually transfers population from the $|\pm 1, g\rangle$ state (via $|\pm 1, e\rangle$ and $|s\rangle$) to the $|0, g\rangle$ state (the $|s\rangle$ state decays almost exclusively to $|0, g\rangle$). Therefore, by simply shining green light on the system and cycling through these transitions the spin population in the ground state is progressively transferred into the $|0\rangle$ spin state. After typically a few microseconds, the system is initialized in the well defined $|0\rangle$ state with a fidelity approaching 95 %.

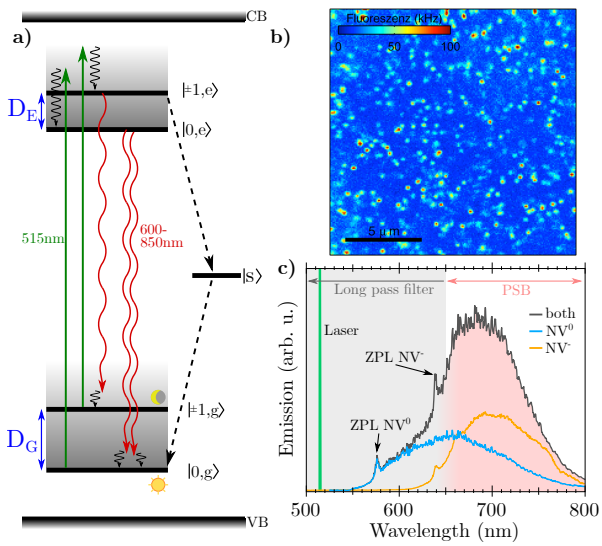

Fig. 2: Photoluminescence of the NV center. a) Simplified energy diagram of the NV center which is situated within the conduction (CB) and valence band (VB) of the diamond lattice. The ground state $|g\rangle$ and the excited state $|e\rangle$ both exhibit a ZFS. Two spin-conserving decay paths are shown after excitation with a green laser ($\lambda \approx 515$ nm), which results in red fluorescence in the bandwidth of $637 - 850$ nm (red curvy arrows) and one indirect spin non-conserving decay path over the metastable state $|s\rangle$, with no photon contributions in the visible spectrum (black dashed arrows). Black curvy arrows denote phonon decays. The $|\pm 1, g\rangle$ states (labelled with the moon) exhibit fewer photons due to an additional decay path over the metastable state, which takes ≈ 300 ns, in contrast to the optical decay (≈ 13 ns). Hence, the $|0, g\rangle$ state (labelled with a sun) appears brighter and produces more photons per unit time. b) Photoluminescence map from a diamond sample with low NV density. Each bright spot corresponds to a single NV center. c) Fluorescence spectrum of NV center upon green laser excitation at room temperature (adapted from [2]). Both charge states of the NV center (with their respective zero-phonon line (ZPL) and PSB) have a different contribution to the overall fluorescence signal. The proper choice of filters allows the spectroscopy to be mainly focused on the NV^- contributions.

1.4 Read-out of the spin-state

The presence of a competing non-radiative decay path for $|\pm 1, e\rangle$ introduces a reduction in the fluorescence count-rate associated with the $|\pm 1\rangle$ spin states. Therefore, by merely monitoring the NV fluorescence count-rate, one can identify the spin state of the system. Hence, the $|0\rangle$ and $|\pm 1\rangle$ states are referred to as the bright and dark state, respectively (indicated with a sun and a moon in Fig. 2b).

1.5 Manipulation of the spin-state

The spin population in the NV center ground state $|g\rangle$ can be further manipulated using a microwave signal resonant to the $|0\rangle \leftrightarrow |\pm 1\rangle$ transition. Fig. 3 shows an example of an optically detected magnetic resonance (ODMR) spectrum, obtained by recording the fluorescence of the NV center as a function of the applied microwave frequency. Away from the spin resonance, the count-rate $\mathcal{R}_0$ corresponds to the NV fluorescence from the bright state $|0\rangle$ (see Fig. 2). When the microwave frequency hits the resonance in Fig. 3a ($\nu_{\mathrm{MW}} = D_G = 2.87\,\mathrm{GHz}$), we observe a reduction in the photon count-rate, corresponding to a transfer of the population from the $|0, g\rangle$ (bright) to the $|\pm 1, g\rangle$ (dark) state. In the case of a continuous wave (CW) excitation the amount of population transferred to the $|\pm 1, g\rangle$ state depends on the microwave (and laser) power. The maximal achievable contrast $\mathcal{C}$ for CW ODMR can reach up to $\sim 30\,\%$ of $\mathcal{R}_0$. To avoid doubt, this number is not a direct consequence of the mentioned branching ratio of 30 %, but rather the outcome of the overall decay rates. The linewidth $\delta\nu$ of the resonance is ultimately limited by the quantum coherence time T_2^* ($\propto 1/\delta\nu$) of the NV center spin states which is usually on the order of µs.

Note, that in the case of a pulsed excitation, the transfer of population can be controlled precisely, and the system can be prepared in any arbitrary superposition of the two states by merely adjusting the pulse length. This property is at the basis of advanced measurement sequences exploiting the full quantum character of the defect, which are not described in the present note. For more details, we refer to the excellent review by Barry J. et al. [3].

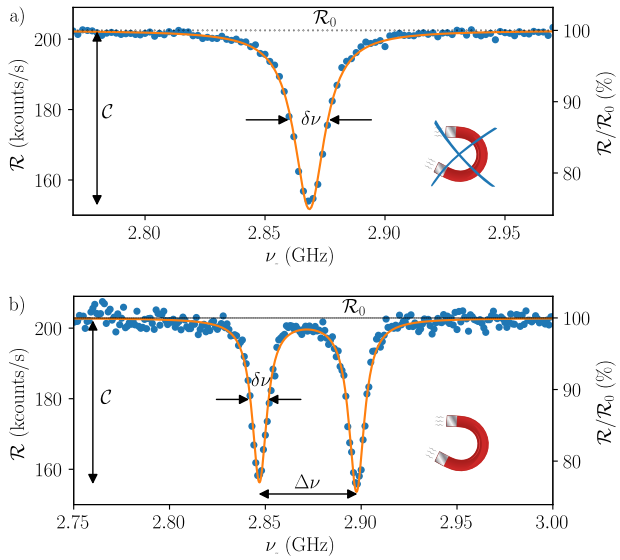

Fig. 3: Optically detected resonance of a NV. a) Fluorescence spectrum of a NV center with the single resonance peak at $\nu_{\mathrm{MW}} = D_G = 2.87\,\mathrm{GHz}$, when no external magnetic field $\boldsymbol{B}$ is applied. b) The two resonances reveal a Zeeman splitting corresponding to $|\boldsymbol{B}| = 1\,\mathrm{mT}$ generated by an external bias magnet. The high photon count-rate ($\mathcal{R}_0 > 200\,\mathrm{kcounts/s}$), large ESR contrast ($\mathcal{C} > 20\,\%$) and narrow linewidth ($\Delta\nu \sim 9\,\mathrm{MHz}$) are typical values for the Quantilever™MX probe, resulting in a sensitivity of $\eta \leq 2.5 \pm 0.1\,\mu\mathrm{T}/\sqrt{\mathrm{Hz}}$.

The NV center in a nutshell

- Only NV^- is used for magnetometry
- Zero-phonon line (ZPL) at 637 nm
- Zero-field splitting (ZFS) is 2.87 GHz
- $\sim 85\,\%$ of the fluorescence decays into the phonon sideband (PSB) 637-850nm
- Maximal contrast of 30 % in CW ODMR
- Green laser initializes and reads out the NV

2 Measuring magnetic fields with the NV center

The susceptibility of the NV center's ground state $|g\rangle$ to a large variety of external fields (magnetic and electric fields, pressure, temperature etc..) makes it a very versatile sensor. In this section we focus on the effect of an external magnetic field and show that the NV center can be turned into a magnetometer with outstanding performance.

2.1 Zeeman effect

The interaction between the NV spin and an external magnetic field $\boldsymbol{B}$ is captured by the fol-

lowing Hamiltonian

$$\mathcal{H}_{\text{int}}/h = \frac{g_e \mu_B}{h}\left(\boldsymbol{B}^\dagger \boldsymbol{S}\right) = \overline{\gamma}_{\text{NV}} \boldsymbol{B}^\dagger \boldsymbol{S}\,, \qquad (1)$$

where $g_e = 2.003$ is the NV electronic Landé factor, μ_B the Bohr magneton, h the Planck's constant and $\boldsymbol{S}^\dagger = (S_x, S_y, S_z)$ the dimensionless electronic spin-1 operator.

Note, that z corresponds to the quantization axis, defined by the axis connecting the nitrogen and the vacancy (green arrow in Fig.1). For convenience, we introduce the reduced NV gyromagnetic ratio $\overline{\gamma}_{\text{NV}} \approx 28\,\text{MHz/mT}$.

Applying a finite static magnetic field $\boldsymbol{B}$ results is a splitting of the $|+1\rangle$ and $|-1\rangle$ spin states known as the Zeeman effect. The Zeeman effect is readily seen on the ODMR spectrum in Fig. 3b, where we observe a lifting of the degeneracy of the $|+1\rangle$ and $|-1\rangle$ spin states and an increase splitting $\Delta\nu$ between the resonance frequencies as the value of the external field $\boldsymbol{B}$ increases.

2.2 Quantitative analysis of the field amplitude

The splitting in frequency is symmetric and directly proportional to the z-component of the magnetic field (i.e the magnetic field along the quantization axis of the NV). The frequency splitting in Fig.3b can be derived from Eq.1 and writes as

$$\Delta\nu = \frac{2 g_e \mu_B}{h} B_z = 2\,\overline{\gamma}_{\text{NV}} B_z. \qquad (2)$$

This equation is remarkable in many ways. First, the relationship between the frequency splitting $\Delta\nu$ and the magnetic field B_z is only dependant on fundamental constants which are the same from one NV center to the next. This property guarantees the reproducibility of a measurement and removes at the same time the need for a sensor calibration. Second, the large value of the prefactor $2\,\overline{\gamma}_{\text{NV}}$ produces measurable frequency shifts even from very small magnetic fields. This is shown in Fig. 3b, where we observe that fields of just a few milli Tesla result in two very distinct spin resonances in the ODMR spectrum. Broadly speaking, Eq. 2 can be applied to small magnetic fields of up to 3 mT (as the non-linear contributions of the perpendicular components are marginal).

In the more general case of a magnetic field with both, axial (B_z) and strong transverse (B_x) components, the splitting is no longer symmetric and the frequencies associated with the $|0\rangle \leftrightarrow |\pm 1\rangle$ transition are given (here up to the third order in α) by

$$\nu_\pm = D\left[1 \pm \left(\alpha\cos\theta_B + \frac{\alpha^2}{2} 3\sin^2\theta_B \pm \alpha^3\left(\frac{1}{8}\sin^3\theta_B \tan\theta_B - \frac{1}{2}\sin^2\theta_B\cos\theta_B\right)\right)\right] \qquad (3)$$

where $\alpha = \overline{\gamma}_{\text{NV}} B/D$ and $\tan\theta_B = B_x/B_z$. By tracking the exact value of both frequencies, the amplitude as well as the orientation of the applied magnetic field can be derived, allowing for a full vector analysis of the external magnetic field.

Magnetometry with the NV center

- Obtain directly the magnetic field via $B_z = \Delta\nu/2\overline{\gamma}_{\text{NV}}$
- $\overline{\gamma}_{\text{NV}} = 28\,\text{MHz/mT}$
- Sensitivity η for CW ODMR: $\sim\mu\text{T}/\sqrt{\text{Hz}}$

2.3 Sensitivity to magnetic fields

CW ODMR with the NV center is the widely employed magnetometry method. The shot-noise limited sensitivity η_{NV} of a NV magnetometer at the steepest slope of the resonance curve (see Fig.

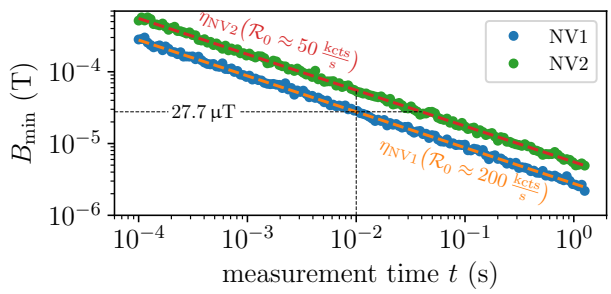

Fig. 4: Sensitivity calculations for two NVs. Two examples (with $\eta_{\text{NV1}} = \eta_{\text{NV2}}/2 = 2.77\,\mu\text{T}/\sqrt{\text{Hz}}$) for the minimal measurable magnetic field $B_{\text{min}} = \eta_{\text{NV}}/\sqrt{t}$ are shown for a shot noise limited configuration (i.e. the detectable magnetic field is limited to the noise originating from counting photons). Improving the sensitivity does not result in a different scaling (it still remains $\propto \sqrt{t}$), but enables to reach a certain value of B_{min} faster (horizontal dashed line) or obtain for a given time t a smaller B_{min} (vertical dashed line).

3) writes as

$$\eta_{\mathrm{NV}}(\mathcal{R}_0, \delta\nu, \mathcal{C}) = B_{\min}(t)\sqrt{t} = \frac{\mathcal{P}_{\mathcal{F}}}{\overline{\gamma}_{\mathrm{NV}}} \frac{\delta\nu}{\mathcal{C}\sqrt{\mathcal{R}_0}}, \quad (4)$$

where $\mathcal{R}_0 = N_{\mathrm{ph}}/t$, $\delta\nu$ and $\mathcal{C}$ corresponds to the count-rate, linewidth and contrast introduced in Fig. 3. The profile factor $\mathcal{P}_{\mathcal{F}}$ captures the shape of the resonance peak which is either of Gaussian ($\mathcal{P}_{\mathcal{F}} = \sqrt{e/(8\ln 2)} \approx 0.70$) or more commonly, of Lorentzian type ($\mathcal{P}_{\mathcal{F}} = 4/(3\sqrt{3}) \approx 0.77$), depending on the laser and microwave excitation power [4]. In the Qnami ProteusQ™, the software is smartly suggesting the choice of parameters for the measurement at hand. Note, that the sensitivity is the ability of an optical magnetometer to resolve a minimal magnetic field $B_{\min}$ in a given time t. Hence, a more (less) sensitive sensor is reflected by a smaller (larger) sensitivity.

To obtain a tangible understanding of Eq. 4 consider Fig. 4, where the smallest detectable field $B_{\min}$ is displayed for two NVs with different count rates $\mathcal{R}_0$. Any improvement in $\mathcal{R}_0 \uparrow, \delta\nu \downarrow$ and $\mathcal{C} \uparrow$ manifests itself in an improved sensitivity $\eta_{\mathrm{NV}} \downarrow$ which enables ultimately the detection of either (i) smaller fields $B_{\min}$, or (ii) the same fields $B_{\min}$, but faster. In the specific example of Fig. 4 we obtain (by improving the count rate by a factor of 4) a $\sqrt{4} = 2$ times smaller sensitivity, and hence 2 times smaller $B_{\min}$ for an integration time of $t = 10$ ms. Or conversely, we obtain the same $B_{\min} \approx 27.7\,\mu\mathrm{T}$ by a factor 4 faster. $B_{\min}$ is ultimately bounded by the overall noise contributions from the environment and will be explored in a further technical note.

2.4 Effect of the magnetic field on the NV fluorescence

Magnetic fields perpendicular to the z-axis (quantization axis) of the defect induce in general a mixing of the $|0\rangle$ and $|\pm1\rangle$ levels in both, the ground $|g\rangle$ and excited states $|e\rangle$. This results in a reduction of the fluorescence signal and the ODMR contrast.

A simulation of the fluorescence response as a function of the magnetic field components $B_\perp$ and B_z is depicted in Fig.5. For a given value of B_z, we observe an overall decrease of the NV fluorescence as the transverse component $B_\perp$ increases [5]. This effect, known as NV fluorescence quenching sets some boundaries to how and with what precision magnetic fields can be measured.

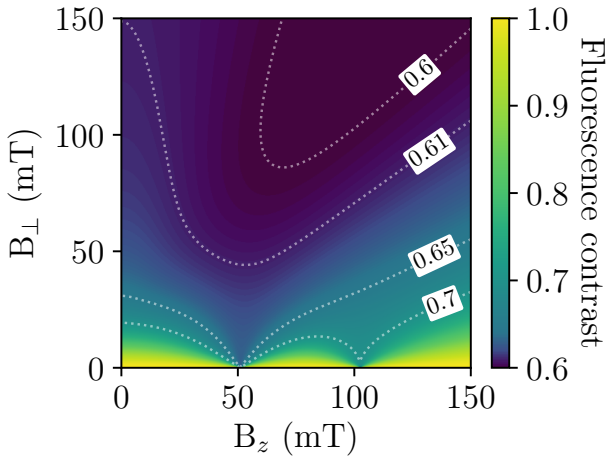

Fig. 5: Impact of magnetic fields on the fluorescence of the NV center. (adapted from Ref. [5]) The two inflection points of the photo luminescence signal seen in the simulation results are attributed to level anti-crossings of the $|0\rangle$ and the $|\pm1\rangle$ spin states (in the excited and the ground state, respectively), caused by the Zeeman interaction with magnetic fields oriented along the quantization axis. The maximal contrast of the quenching imaging mode is on the order of 40 %.

On the one hand, quenching of the NV fluorescence is accompanied by a reduction of the contrast in the ODMR signal, thereby reducing effectively the sensitivity (see Eq. 4). On the other hand, monitoring the changes in the fluorescence count rate provides an indication on the variation of the magnetic field. While less precise than the approach based on ODMR, we obtain with the quenching measurement a fast qualitative overview of the magnetic field fluctuations in a sample. In addition, it does not require external controls for RF field or a static bias magnetic field (which is necessary for ODMR measurements).

The details and specifics of quenching and ODMR measurements will be covered in a separate technical note, but we highlight here some general principles to guide the user:

Measurement mode guideline

- $\mu\mathrm{T} \lesssim |\boldsymbol{B}| \lesssim 5\,\mathrm{mT}$: ODMR applies (regions in the color yellow to light green)
- $3\mathrm{mT} \lesssim |\boldsymbol{B}| \lesssim 50\,\mathrm{mT}$: quenching applies (regions in the light green to light blue)
- $|\boldsymbol{B}| \gtrsim 50\,\mathrm{mT}$: special techniques required (e.g. application of external bias field)

References

[1] M. W. Doherty, N. B. Manson, et al., "The nitrogen-vacancy colour centre in diamond", Physics Reports **528**, 1–45 (2013).

[2] J. Jeske, D. W. M. Lau, et al., "Stimulated emission from nitrogen-vacancy centres in diamond", Nature Communications **8** (2017).

[3] J. F. Barry, J. M. Schloss, et al., "Sensitivity optimization for NV-diamond magnetometry", Reviews of Modern Physics **92** (2020).

[4] A. Dréau, M. Lesik, et al., "Avoiding power broadening in optically detected magnetic resonance of single NV defects for enhanced dc magnetic field sensitivity", Physical Review B **84** (2011).

[5] J.-P. Tetienne, L. Rondin, et al., "Magnetic-field-dependent photodynamics of single NV defects in diamond", New Journal of Physics **14**, 103033 (2012).

Address Qnami AG
Hofackerstrasse 40B
4132 Muttenz
Switzerland

Website www.qnami.ch